

DOI: 10.1002/((please add manuscript number))

Article type: Communication

Insight into Ca-substitution effects on O3-type $\text{NaNi}_{1/3}\text{Fe}_{1/3}\text{Mn}_{1/3}\text{O}_2$ cathode materials for sodium ion batteries application

Liqi Sun#, Yingying Xie#, Xiao-Zhen Liao, Hong Wang, Guoqiang Tan, Zonghai Chen, Yang Ren, Jihyeon Gim, Wan Tang, Yu-Shi He, Khalil Amine, Zi-Feng Ma*

L. Sun, Y. Xie, Dr. X.-Z. Liao, H. Wang, W. Tang, Y.-S. He, Prof. Z.-F. Ma

Department of Chemical Engineering

Shanghai Jiao Tong University

Shanghai 200240, China

E-mail: liaoxyz@sjtu.edu.cn

Dr. Z. Chen, Dr. G. Tan, Dr. J. Gim, Dr. K. Amine

Chemical Sciences and Engineering Division

Argonne National Laboratory

9700 South Cass Avenue, Lemont, IL 60439, USA

Dr. Y. Ren

Advanced Photon Source

Argonne National Laboratory

9700 South Cass Avenue, Lemont, IL 60439, USA

Keywords: layered sodium transition metal oxide, sodium ion battery, Ca-substitution

Abstract

O3-type $\text{NaNi}_{1/3}\text{Fe}_{1/3}\text{Mn}_{1/3}\text{O}_2$ (NaNFM) has been well investigated as promising cathode material for sodium ion batteries, but the cycling stability of NaNFM still need to be improved by using novel electrolytes or optimizing their structure with the substitution of different elements sites. To enlarge alkali-layer distance inside the layer structure of NaNFM might benefit Na^+ diffusion. In this communication, we first report the effect of Ca-substitution in Na sites on the structural and electrochemical properties of $\text{Na}_{1-x}\text{Ca}_{x/2}\text{NFM}$ ($x=0, 0.05, 0.1$). X-ray diffraction patterns of the prepared $\text{Na}_{1-x}\text{Ca}_{x/2}\text{NFM}$ samples show single $\alpha\text{-NaFeO}_2$ type phase with slightly increased alkali-layer distance as Ca content increased. The cycling stabilities of Ca-substituted samples are remarkably improved. The $\text{Na}_{0.9}\text{Ca}_{0.05}\text{NFM}$ cathode delivers capacity of 116.3 mAh g^{-1} with capacity retention of 92% after 200 cycles at 1C rate. In operando XRD indicates a reversible structural evolution

through an O3-P3-P3-O3 sequence of $\text{Na}_{0.9}\text{Ca}_{0.05}\text{NFM}$ cathode during cycling. Compared to NaNMF , the $\text{Na}_{0.9}\text{Ca}_{0.05}\text{NFM}$ cathode show wider voltage range in pure P3 phase state during charge/discharge process, and exhibits better structure recoverability after cycling. The superior cycling stability of $\text{Na}_{0.9}\text{Ca}_{0.05}\text{NFM}$ makes it a promising material for practical applications in sodium ion batteries.

Sodium ion batteries (SIBs) are attracting great interest for large-scale energy storage applications due to the natural abundance and low cost of sodium resources. The development of high performance electrode materials is one of the key projects for SIB technique. Various cathode materials for SIBs have been studied such as layered transition metal oxides Na_xMO_2 (M = one or more transition metal elements),^[1-14] poly-anionic networks^[15-17] and prussian blue analogues.^[18-21] Layered sodium transition metal oxides especially the mixture transitional metal oxides have been intensively studied as desirable cathode materials for SIBs due to their easy synthesis and attractive electrochemical performance.

Sodium transition metal oxides Na_xMO_2 are characterized with typical layered structure built by edge-sharing MO_6 octahedral units forming MO_2 -sheets, and the sodium cations coordinated in the octahedral (O), tetrahedral (T), or prismatic (P) sites between the MO_2 -sheets.^[1] Among these Na_xMO_2 phases, O3 and P2 type $\text{Na}_x(\text{Fe},\text{Mn},\text{M}')\text{O}_2$ compounds have attracted great interest due to the low cost and environment friendly of Mn and Fe, and the attractive sodium ion intercalation behavior. O3 phase has the advantage of accommodating higher amount Na-ion into the layered structure and shows higher charge/discharge capacity compared to P2 phase, but with low stability.^[2,4,5,23] The P2 Phase materials have been demonstrated to have superior Na-ion conductivity to O3 phase and present better rate capacity and cycle performance.^[24,25] It is worth to explore more proper methods to improve the cycling performance of O3 phase materials.

O3-type layered $\text{NaNi}_{1/3}\text{Fe}_{1/3}\text{Mn}_{1/3}\text{O}_2$, which was first reported by Johnson C. S. et al,^[4] is one of the most promising positive electrode candidates with appreciable capacity of 130 mAh g⁻¹ (0.1C) and easy to synthesis. The structural change and reaction mechanism during the sodium intercalation/deintercalation process of $\text{NaNi}_{1/3}\text{Fe}_{1/3}\text{Mn}_{1/3}\text{O}_2$ cathode was investigated by using in operando XRD and TXM technique.^[26] In this work, we report the remarkably improved cycle stability of Ca-substituted $\text{Na}_{0.9}\text{Ca}_{0.05}\text{Ni}_{1/3}\text{Fe}_{1/3}\text{Mn}_{1/3}\text{O}_2$ ($\text{Na}_{0.9}\text{Ca}_{0.05}\text{NFM}$) sample. Ca-substitution enlarged alkali-layer distance of the layered structure. The Ca-substituted $\text{Na}_{1-x}\text{Ca}_{x/2}\text{NFM}$ ($x=0, 0.05, 0.10$) samples were synthesized by solid-state reaction method. **Figure 1a-c** Show the FSEM images of the as prepared $\text{Na}_{1-x}\text{Ca}_{x/2}\text{NFM}$ ($x=0, 0.05, 0.1$) sample powders. All $\text{Na}_{1-x}\text{Ca}_{x/2}\text{NFM}$ samples showed a distribution of spherical secondary particles in the range of 3-10 μm . The micron size spheres were agglomerated with plate like primary particles with typical diameter size between 0.2-0.8 μm and thickness about 0.1-0.3 μm . The elemental compositions of the sample materials were measured by ICP-OES, which were $\text{Na}_{0.991}\text{Ni}_{0.321}\text{Fe}_{0.321}\text{Mn}_{0.325}\text{O}_x$, $\text{Na}_{0.959}\text{Ca}_{0.024}\text{Ni}_{0.316}\text{Fe}_{0.326}\text{Mn}_{0.320}\text{O}_x$ and $\text{Na}_{0.912}\text{Ca}_{0.048}\text{Ni}_{0.320}\text{Fe}_{0.333}\text{Mn}_{0.330}\text{O}_x$ respectively. The Na:Ca:Ni:Mn:Fe mole ratios were consistent with the as-designated compositions for $\text{Na}_{1-x}\text{Ca}_{x/2}\text{Ni}_{1/3}\text{Fe}_{1/3}\text{Mn}_{1/3}\text{O}_2$ ($x=0, 0.05$ and 0.10) samples, within the error of the determination. Therefore we simply refer the as-prepared samples as $\text{Na}_{1-x}\text{Ca}_{x/2}\text{NFM}$ ($x=0, 0.05$ and 0.10) in the context. The crystal structures of the $\text{Na}_{1-x}\text{Ca}_{x/2}\text{NFM}$ ($x= 0, 0.05, 0.10$) materials were characterized by synchrotron x-ray powder diffraction. Powder XRD patterns shown in **Figure 1d** demonstrate that all samples present single phase which can be indexed to R-3m space group with the α - NaFeO_2 structure. Crystal structure of the samples were further refined using the powder profile refinement program GSAS based on initial structural model of α - NaFeO_2 . Cation mixing between Na^+ (Ca^{2+}) and transition metal ions was not considered in the refinement due to the relatively large difference between the ionic radii of Na^+ (Ca^{2+}) and transition metal ions. **Figure S1** show the refined patterns and the Rietveld results were list in

Table S1. The Ca-substituted samples showed increased c-axis length due to the increase of Na⁺ vacancies caused by Ca²⁺ substitution. The Na_{0.9}Ca_{0.05}NMF and Na_{0.95}Ca_{0.025}NMF samples show a O-Na-O layer thickness of 3.272 Å and 3.239 Å, respectively, compared to the 3.235 Å of pristine NaNMF. The increased O-Na-O layer thickness may benefit the Na⁺ diffusion.

The difference lying in crystalline structure between Na_{0.9}Ca_{0.05}NMF and pristine NaNMF was further characterized by the transmission electron microscopy (TEM), as shown in **Figure 2**. For the pristine NaNMF sample, the high-resolution TEM image in **Figure 2A** displays highly ordered lattices spaced by 2.6 Å, corresponding to the (101) planes of layered NaNMF. This finding well matched with the XRD results. **Figure S2** exhibits particle morphology and its elemental composition of NaNMF by energy dispersive X-ray spectroscopy (EDXS). The EDXS mapping shows uniform elemental distribution of Na, Ni, Mn, Fe and O throughout the entire particle, indicating uniform chemical composition in the material bulk. Comparatively, the Na_{0.9}Ca_{0.05}NMF (**Figure 2B**) exhibits a changed structural characteristic that the lattice d spacing of the (101) was expanded to 2.8 Å. This is considered to be most solid evidence to confirm that the Ca ions have really doped into the material bulk. **Figure 2C** shows a single particle sized of ~ 800 nm for the Na_{0.9}Ca_{0.05}NMF. The EDXS mapping reveals that the particle also has uniform elemental composition. In addition, the EDXS elemental profile displays the atomic proportion of each element, where the atomic ratio of Ni, Mn, and Fe is approximate 1.0 : 1.1 : 1.2, which is closed to the value of stoichiometric formula. The above finding well matched with the XRD results.

Electrochemical properties of the Na_{1-x}Ca_{x/2}NFM (x=0, 0.05, 0.1) cathodes were evaluated in the voltage range of 2.0-4.0V using CR2016 coin cells with Na foil as anode. **Figure 3a** shows the initial galvanostatic charge/discharge profiles of the prepared cells at a current density of 13 mA g⁻¹ (0.1C). It can be seen that the NaNMF sample showed the largest capacity of 130.2 mAh g⁻¹, while the Na_{1-x}Ca_{x/2}NFM (x= 0.05, 0.1) samples show slightly

decreased discharge capacities of 129.0 mAh g⁻¹ and 126.9 mAh g⁻¹, respectively. After 2 cycles charge/discharge at 13 mA g⁻¹, the cells were cycled using current density of 130 mAh g⁻¹ (1C) for 200 cycles. **Figure 3b** presents the first charge/discharge profiles at 1C rate. **Figure 3a&b** show that the discharge profiles of all the samples present similar characteristic with two typical procedures as marked by AB and BC segments. The AB segment corresponds to a one phase process, and the BC segment corresponds to a two phases transition process. The discharge profiles of all the samples overlap well at AB segment indicating a similar electronic and sodium ion transfer capabilities at low Na⁺ content state. The different discharge behavior of the samples mainly demonstrated on BC segment. Ca-substituted samples Na_{0.95}Ca_{0.025}NFM and Na_{0.9}Ca_{0.05}NFM showed slightly decreased capacities of 120.0mAh g⁻¹ (1C) and 116.1 mAh g⁻¹ (1C), respectively, compared with the pristine NaNMF (122.0mAh g⁻¹). The decreased capacities of the Ca-substituted samples maybe due to the inactivity of Ca²⁺ in the insertion/extraction process (discussed in the following section). However, the comparison of long term cycling behaviors of the Na_{1-x}Ca_{x/2}NFM samples in 1C rate charge/discharge as presented in **Figure. 3c** show interesting results. Although the NaNMF cathode showed highest primary capacity of 122.0 mAh g⁻¹, the capacity retention after 200cycles was 67%. On the other hand, the Na_{0.9}Ca_{0.05}NFM sample delivered lowest primary discharge capacity of 116.1mAh g⁻¹ due to the high content of Ca²⁺. It exhibited excellent cycling stability with capacity retention of 91.8% after 200 cycles. The Na_{0.95}Ca_{0.025}NFM presented medium performance with primary capacity of 120.0mAh g⁻¹ and capacity retention of 74.6% after 200 cycles. The above results indicate that proper amount of Ca²⁺ substitution can remarkably improve long term cycling stability of the NaNMF sample. Actually, further increase the Ca²⁺ content may cause decrease of specific capacity of the sample material. **Figure S3** compared the cycling performance of a higher Ca²⁺ content sample Na_{0.85}Ca_{0.075}NFM with that of Na_{0.9}Ca_{0.05}NFM. It is clear that the Na_{0.85}Ca_{0.075}NFM sample only delivered a discharge capacity of 109.2 mAh g⁻¹ with similar long term cycling

stability as $\text{Na}_{0.9}\text{Ca}_{0.05}\text{NFM}$ sample at 1C rate. $\text{Na}_{0.9}\text{Ca}_{0.05}\text{NFM}$ shows the best cycling performance in this work.

Figure 3d further compared the rate capabilities of the $\text{Na}_{1-x}\text{Ca}_{x/2}\text{NFM}$ ($x=0, 0.05, 0.1$) electrodes. The charge/discharge tests were performed galvanostatically in the voltage window of 2.0-4.0V under different current densities, ranging from 13 mA g^{-1} (0.1C) up to 1300 mA g^{-1} (10 C). The NaNMF delivered rate capacities of 130.4 mAh g^{-1} (0.1C), 122.2 mAh g^{-1} (1C), 115.4 mAh g^{-1} (2C), 103.9 mAh g^{-1} (5C) and 83.2 mAh g^{-1} (10C), respectively. It worth noticed that Ca-substituted $\text{Na}_{1-x}\text{Ca}_{x/2}\text{NFM}$ ($x= 0.05, 0.1$) samples show only slightly lower capacities than NaNMF at 0.1C, 1C and 2C rate. The discharge capacities of $\text{Na}_{1-x}\text{Ca}_{x/2}\text{NFM}$ ($x= 0.05, 0.1$) at 5C, 10C rates were similar to those of NaNMF. The $\text{Na}_{0.9}\text{Ca}_{0.05}\text{NFM}$ electrode delivered capacities of 127.4 mAh g^{-1} (0.1C), 116.3 mAh g^{-1} (1C), 110.2 mAh g^{-1} (2C), 102.1 mAh g^{-1} (5C) and 86.2 mAh g^{-1} (10C), respectively.

In order to clarify whether Ca^{2+} is electrochemically insertion/extraction active, we performed XPS analysis on the charged $\text{Na}_{0.9}\text{Ca}_{0.05}\text{NFM}$ cathode (at 4V state) and compared with uncycled $\text{Na}_{0.9}\text{Ca}_{0.05}\text{NFM}$ electrode. **Figure S4** shows the Na1s and Ca2p XPS spectra. It is clear that the charged $\text{Na}_{0.9}\text{Ca}_{0.05}\text{NFM}$ electrode showed obviously decreased intensity of Na1s spectrum compared with uncycled $\text{Na}_{0.9}\text{Ca}_{0.05}\text{NFM}$ electrode due to the extraction of Na^+ in the charge process. However, there is no noticeable difference on the Ca2p XPS spectra between uncycled and charged $\text{Na}_{0.9}\text{Ca}_{0.05}\text{NFM}$ electrodes. This observation may indicate that Ca^{2+} is not extracted from the crystal structure. To further confirm this observation, the variation in chemical composition of the $\text{Na}_{0.9}\text{Ca}_{0.05}\text{NFM}$ electrode after charged to 4.0V was measured via ICP test. The powder materials scraped from pristine $\text{Na}_{0.9}\text{Ca}_{0.05}\text{NFM}$ electrode and charged $\text{Na}_{0.9}\text{Ca}_{0.05}\text{NFM}$ electrode (4V) were soaked and stirred in hot nitric acid for 1h, respectively, to dissolve the $\text{Na}_x\text{Ca}_y\text{NFM}$ compounds. The nitrate solutions were cooled and filtered, and then used for ICP measurement. The ICP results of the pristine and charged $\text{Na}_{0.9}\text{Ca}_{0.05}\text{NFM}$ electrodes were $\text{Na}_{0.842}:\text{Ca}_{0.039}$:

$\text{Ni}_{0.296}\text{Fe}_{0.372}\text{Mn}_{0.332}$ and $\text{Na}_{0.401}\text{Ca}_{0.037}\text{Ni}_{0.299}\text{Fe}_{0.382}\text{Mn}_{0.319}$, respectively. It is obvious that the charged electrode showed obviously decreased Na^+ content and almost the same Ca^{2+} content compared with the pristine $\text{Na}_{0.9}\text{Ca}_{0.05}\text{NFM}$ electrode. Thus, we conclude that Ca^{2+} is inactive during the electrochemical cycling. However, the existence of immobile Ca^{2+} in sodium layer may cause influence on the sodium diffusion and evolution of the crystal structure during charge and discharge process.

In situ XRD analysis was performed to understand the structure evolution and sodium extraction/insertion behavior of Ca-substituted $\text{Na}_{0.9}\text{Ca}_{0.05}\text{NFM}$. **Figure 4** displays the in-situ XRD patterns and corresponding charge-discharge curve of $\text{Na}_{0.9}\text{Ca}_{0.05}\text{NFM}$ electrode during the first charge-discharge cycle in the voltage range of 2.0-4.0V. It can be seen that the initial XRD diffraction peaks could be well indexed to the space group R-3m with O3 phase hexagonal layered structure, and all the peaks belong to O3 phase begin to change along with the charge proceeding. With the increase of charge voltage, the (003), (006), (107) and (018) peaks shift to lower angles, the intensity of (104) peak decreases and the position shifts to higher angles. When the charge voltage increases to 2.97V, the (006), (101), (012), and (110) peaks split into two and some new peaks that can be assigned to a hexagonal P3 phase start to appear, indicating that P3 phase appears at 2.97V and a two-phase reaction with the coexistence of O3 and P3 phases in the voltage range of 2.97–3.15 V. After 3.15V, all the peaks belong to O3 phase disappeared and the remaining P3 phase maintains till the charging proceeding finished at 4.0V. During the discharge process, the XRD patterns indicate a reversible phase transformation compared with charge process. P3 phase keeps stable in a long time till 2.75V. Then some new peaks indexed to O3 phase appeared, such as O3 (003) and (006) appeared at the right of P3 (003) and (006) peaks. With the proceeding of discharge, all the other peaks also were shifting to the initial position. After discharge to 2.58v, almost all the P3 phase peaks disappeared, and the O3 peaks shifted to the initial position along with the discharge proceeded. The XRD pattern indicate a reversible “O3-P3-P3-O3” phase

transformation during the charge and discharge process just like the phase transition characteristic of NaNFM that we have demonstrated in reference 26 (shown in **Figure S5**). It is clear that the $\text{Na}_{0.9}\text{Ca}_{0.05}\text{NFM}$ sample exhibited a wider voltage range (3.15V \rightarrow 4.0V \rightarrow 2.75V) in pure P3 state, compared to that of pristine NaNMF (3.5 \rightarrow 4.0V \rightarrow 2.8V). The detail change of lattice parameters of $\text{Na}_{0.9}\text{Ca}_{0.05}\text{NFM}$ during cycling was determined by using Fullprof software (**Table S2**, Supporting Information). **Table S2** demonstrates that the lattice parameter a and c show very good reversible change in the charge-discharge process. The in-situ XRD pattern at 2.0V discharge state show good recovery compared to the XRD pattern of precycled electrode. Compared with the in situ XRD pattern of pristine NaNMF in **Figure S5**, The $\text{Na}_{0.9}\text{Ca}_{0.05}\text{NFM}$ show wider voltage range in P3 phase and exhibit better structure recoverability. These may attribute to the excellent cycling stability of $\text{Na}_{0.9}\text{Ca}_{0.05}\text{NFM}$ electrode.

To further understand the electrode kinetics on sodium insertion/extraction process of the Ca-substituted materials, the cyclic voltammograms of the $\text{Na}_{1-x}\text{Ca}_{x/2}\text{NFM}$ electrodes in potential range of 2.0-4.0V vs. Na^+/Na at varied scan rates were measured. The apparent Na diffusion coefficients (D) of $\text{Na}_{1-x}\text{Ca}_{x/2}\text{NFM}$ (x=0, 0.05, 0.10) electrodes were determined by CV results. The CV profiles shown in **Figure 5** display two pairs of reversible redox peaks, corresponding to the two-stage mechanism for sodium extraction and insertion as shown in the charge/discharge profiles in **Figure 3a&b**, which are connected with the O3-P3 transform process at lower voltage range and homogenous P3 phase process at higher voltage range. The redox peaks in the lower voltage range represent the sodium ion extraction/insertion behavior in rich Na^+ state of the bulk material, and the corresponding I_p values show a good linear dependence on the square root of scan rate ($V^{1/2}$) during both charge and discharge procedures as shown in **Figure 5d&e**, indicating a diffusion controlled behavior. The sodium diffusion coefficients can be calculated based on the Randles-Sevcik equation: ^[27,28]

$$I_p = 2.69 \times 10^5 n^{3/2} A D^{1/2} v^{1/2} C_0$$

Where n is the electron transfer number of the reaction, A is the surface area of the electrode, D is the apparent diffusion coefficient of Na^+ and C_0 is the concentration of Na^+ in the lattice. The obtained sodium ion diffusion coefficients were listed in **Table 1**. It is interesting to find that all the samples show very small difference on Na^+ diffusion coefficient both for charge and discharge process. This result well explain the similar high rate capabilities of the Ca-substituted materials with the pristine NaNMF as shown in **Figure 3d**. The $\text{Na}_{0.9}\text{Ca}_{0.05}\text{NFM}$ sample exhibited slightly larger D value for Na^+ extraction compared with pristine NaNMF. This might be explained by the enlarged Na^+ layer distance caused by Ca^{2+} substitution and also the remain of Ca^{2+} between the negative MO_6 layers during Na^+ extraction process may benefit the stability of the crystal structure. However, the D value for Na^+ insertion of $\text{Na}_{0.9}\text{Ca}_{0.05}\text{NFM}$ was slightly lower than NaNMF, though the value difference is negligible. This might be due to the barrier and repulsive effects of immobile Ca^{2+} ions to the inserting Na^+ ions. It is worth mention that the Ca-substituted samples only show slightly decreased specific capacities in lower current densities due to the lower Na^+ content in the material composition, their high rate performances were not inferior to the pristine NaNMF. Anyway, the remarkably improved cycling stability of $\text{Na}_{0.9}\text{Ca}_{0.05}\text{NFM}$ make it a promising cathode material for practical application.

In conclusion, Ca-substitution on the alkaline layer of $\text{NaNi}_{1/3}\text{Fe}_{1/3}\text{Mn}_{1/3}\text{O}_2$ has been explored. $\text{Na}_{1-x}\text{Ca}_{x/2}\text{Ni}_{1/3}\text{Fe}_{1/3}\text{Mn}_{1/3}\text{O}_2$ ($x=0, 0.05, 0.10$) were synthesized and investigated. XRD analyses indicated that Ca-substituted samples kept the same O3 type crystal structure of pristine NaNMF with slightly enlarged d -spacing of the alkaline layer. In situ XRD demonstrated a reversible “O3-P3-P3-O3” phase transformation of $\text{Na}_{0.9}\text{Ca}_{0.05}\text{NFM}$ during the charge and discharge process. Ca-substitution widen the voltage range of P3 phase and $\text{Na}_{0.9}\text{Ca}_{0.05}\text{NFM}$ also showed very good structure recoverability after the charge-discharge cycling. The $\text{Na}_{0.9}\text{Ca}_{0.05}\text{NFM}$ cathode exhibited remarkably enhanced cycling stability with

initial 1C rate reversible capacity of 116.3 mAh g⁻¹ and capacity retention of 92% after 200 cycles. The Na_{0.9}Ca_{0.05}NFM cathode delivered capacities of 102.1 mAh g⁻¹ (5C) and 86.2 mAh g⁻¹ (10C) with capacity retention of 92% (1C) after 200 cycles, The superior cycling stability and good rate performance of Na_{0.9}Ca_{0.05}NFM makes it a promising material for practical applications in SIBs.

Experimental Section

The Ca-substituted Na_{1-x}Ca_{x/2}Ni_{1/3}Fe_{1/3}Mn_{1/3}O₂ (x=0, 0.05, 0.10) samples were synthesized by solid-state reaction method using stoichiometric amount of transition metal hydroxide Ni_{1/3}Fe_{1/3}Mn_{1/3}(OH)₂, Na₂CO₃, CaCO₃ and 2wt.% excess of Na₂CO₃ precursors. The precursor mixtures were calcined at 550 °C for 6 hours, followed by 875 °C annealing in air for 18h to obtain final products. The chemical composition of the sample materials was examined by inductively coupled plasma analysis (ICP, iCAP 6000 Radial, Thermo Fisher Scientific Inc.) The morphology of the samples was observed by Field emission scanning electron microscopy (FESEM, Nova NanoSEM 450 FEI Company). TEM and EDXS were performed using an aberration-corrected JEOL JEM-ARM 200CF STEM equipped with a 200 keV cold-field emission gun, with a HAADF detector and an Oxford X-max 80 SDD X-ray detector.

The structural characteristic of the as-prepared materials was determined by high-energy X-ray diffraction (HEXRD) carried out at beamline11-ID-C of the Advanced Photon Source at Argonne National Laboratory. The wavelength of the X-ray beam used was 0.1173 Å. Crystal structures were refined using the powder profile refinement program GSAS. In situ synchrotron X-ray diffraction (XRD) measurements were performed to analyze the structure evolution of the Na_{0.9}Ca_{0.05}NFM cathode. The in situ HEXRD of Na_{0.9}Ca_{0.05}NFM cathode during cycling was also performed at sector 11-ID-C of the APS at Argonne National Laboratory with the wavelength of the X-ray beam 0.1173 Å. Coin cells with holes for beam

pass were used. The holes at the top and bottom cases of the coin-cell were sealed with Kapton tape after cell assembly.

For electrochemical tests, the cathodes were prepared by slurring 80 wt.% cathode material, 10wt.% super P, and 10wt.% polyvinylidene difluoride (PVDF) binder in N-methyl-2-pyrrolidone (NMP) solvent, and then casting the mixture onto an aluminum foil. After drying at 100°C for about 2h, the electrode disks (14 mm) were punched. After further drying under vacuum at 120 °C for 12 h, the cathodes were incorporated into coin cells (R2016) with sodium metal foil and 1.0M NaClO₄/PC+EMC+FEC (50:48:2, v/v/v) electrolyte in an argon filled glove box. The mass loading of active materials on cathodes was about 4.3 mg cm⁻². The galvanostatic charge-discharge tests of the coin cells were conducted using a battery test system (Land CT2001A model, Wuhan Jinnuo Electronics Co., Ltd.). The cyclic voltammetric (CV) measurements were carried out on CHI electrochemical workstation (CHI 604D, CHI Instrument Co.).

Supporting Information

Supporting Information is available from the Wiley Online Library or from the author.

Acknowledgements

This work was supported by the Natural Science Foundation of China (21573147, 21506123 and 21676165), the National Key Research and Development Program (2016YFB0901500) and Natural Science Foundation of Shanghai (15ZR1422300). This research used resources of the Advanced Photon Source, a U. S. Department of Energy (DOE) Office of Science User Facility operated for the DOE Office of Science by Argonne National Laboratory.

Liqi Sun and Yingying Xie contributed equally to this work.

References

- [1] C. Delmas, J.J. Braconnier, C. Fouassier and P. Hagenmuller, *Solid State Ionics*, **1981**, 3, 165.
- [2] N. Yabuuchi, M. Kajiyama, J. Iwatate, H. Nishikawa, S. Hitomi, R. Okuyama, R. Usui, Y. Yamada and S. Komaba, *Nat. Mater.*, **2012**, 11, 512.
- [3] X. Ma, H. Chen and G. Ceder, *J. Electrochem. Soc.*, **2011**, 158, A1307.
- [4] D. Kim, E. Lee, M. Slater, W. Lu, S. Rood and C.S. Johnson, *Electrochem. Commun.*, **2012**, 18, 66.
- [5] Z. Lu and J.R. Dahn, *J. Electrochem. Soc.*, **2001**, 148, A1225.
- [6] L. Mu, S. Xu, Y. Li, Y. S. Hu, H. Li, L. Chen and X. Huang, *Adv. Mater.*, **2015**, 27, 6928.
- [7] P. Vassilaras, X. Ma, X. Li and G. Ceder, *J. Electrochem. Soc.*, **2013**, 160, A207.
- [8] S. M. Oh, S. T. Myung, C. S. Yoon, J. Lu, J. Hassoun, B. Scrosati, K. Amine and Y. K. Sun, *Nano Lett.*, **2014**, 14, 1620.
- [9] S. H. Guo, P. Liu, Y. Sun, Kai. Zhu, J. Yi, M. Chen, M. Ishida and H. S. Zhou, *Angew. Chem. Int. Ed.*, 2015, 54, 11701.
- [10] H. Wang, B. Yang, X. Z. Liao, J. Xu, D. Yang, Y. He and Z. F. Ma, *Electrochim. Acta*, **2013**, 113, 200.
- [11] X. Xia and J.R. Dahn, *J. Electrochem. Soc.*, **2012**, 159, A1048.
- [12] D. Buchholz, L. G. Chagas, M. Winter and S. Passerini, *Electrochim. Acta*, **2013**, 110, 208.
- [13] I. Hasa, D. Buchholz, S. Passerini, B. Scrosati and J. Hassoun, *Adv. Energy Mater.*, **2014**, 4, 83.
- [14] Y. Wang, R. Xiao, Y. S. Hu, M. Avdeev and L. Q. Chen, *Nat. Mater.*, **2015**, 6, 6954.
- [15] J. Gopalakrishnan and K.K. Rangan, *Chem. Mater.*, **1992**, 4, 745.

- [16] Z. Jian, L. Zhao, H. Pan, Y. S. Hu, H. Li, W. Chen and L. Chen, *Electrochem. Commun.*, **2012**, *14*, 86.
- [17] Z. Li, Dorthe B. Ravnsbæk, K. Xiang, Y. M. Chiang, *Electrochem. Commun.*, **2014**, *44*, 12.
- [18] X. Wu, W. Deng, J. Qian, Y. Cao, X. Ai and H. Yang, *J. Mater. Chem. A*, **2013**, *1*, 10130.
- [19] C. D. Wessells, R. A. Huggins and Y. Cui, *Nat. Commun.*, **2011**, *2*, 550.
- [20] J. Song, L. Wang, Y. Lu, J. Liu, B. Guo, P. Xiao, J. J. Lee, X. Q. Yang, G. Henkelman and J. B. Goodenough, *J. Am. Chem. Soc.*, **2015**, *137*, 2658.
- [21] D. Yang, J. Xu, X. Z. Liao, H. Wang, Y. S. He and Z. F. Ma, *Chem. Commun.*, **2015**, *51*, 8181.
- [22] I. Hasa, D. Buchholz, S. Passerini and J. Hassoun, *ACS Appl. Mater. Interfaces*, **2015**, *7*, 5206.
- [23] J. Y. Hwang, S. T. Myung, D. Aurbach and Y. K. Sun, *J. Power Sources*, **2016**, *324*, 106.
- [24] Y. Li, Z. Yang, S. Xu, L. Mu, L. Gu, Y. S. Hu, H. Li and L. Chen, *Adv. Sci.*, **2015**, *2*, 1500031.
- [25] X. Wang, M. Tamaru, M. Okubo and A. Yamada, *J. Phys. Chem. C*, **2013**, *117*, 15545.
- [26] Y. Xie, H. Wang, G. Xu, J. Wang, H. Sheng, Z. Chen, Y. Ren, C. J. Sun, J. Wen, J. Wang, D. J. Miller, J. Lu, K. Amine and Z. F. Ma, *Adv. Energy Mater.*, **2016**, *6*, 1601306.
- [27] J.-L. Yue, Y.-N. Zhou, X. Yu, S.-M. Bak, X.-Q. Yang, Z.-W. Fu, *J. Mater. Chem. A* **2015**, *3*, 23261
- [28] W. L. Pang, X. H. Zhang, J. Z. Guo, J. Y. Li, X. Yan, B.H. Hou, H. Y. Guan, X. L. Wu, *J. Power Sources* **2017**, *356*, 80.

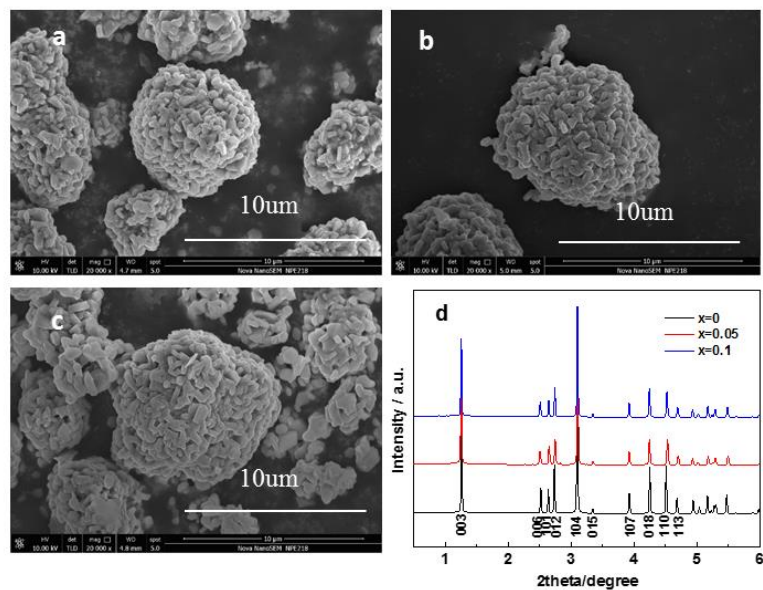


Figure 1. FSEM images and X-ray diffraction patterns of the prepared $\text{Na}_{1-x}\text{Ca}_{x/2}\text{NFM}$ ($x=0, 0.05, 0.10$) samples

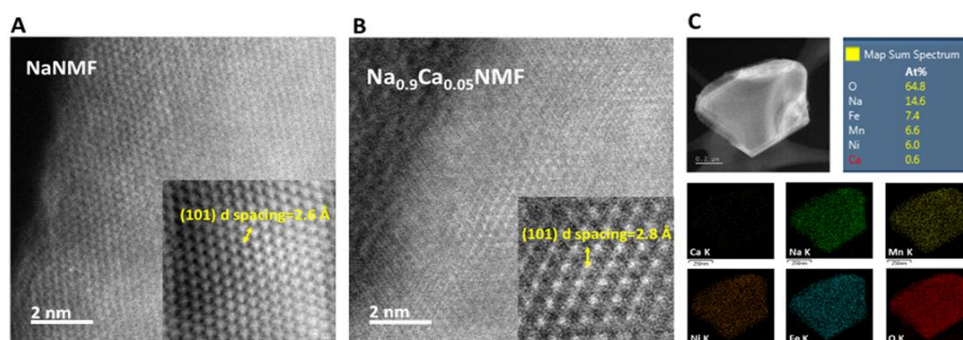


Figure 2. HRTEM images of (a) NaNMF and (b) $\text{Na}_{0.9}\text{Ca}_{0.05}\text{NMF}$ and EDXS mapping results of $\text{Na}_{0.9}\text{Ca}_{0.05}\text{NMF}$ (c)

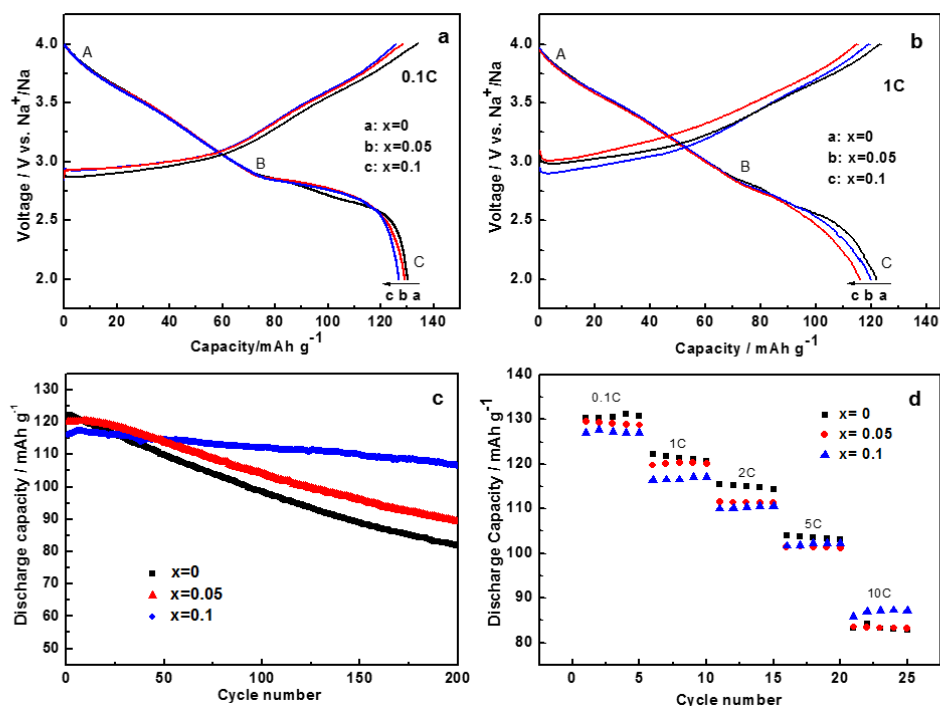


Figure 3. The first charge/discharge profiles of Na_{1-x}Ca_{x/2}NFM (x=0, 0.05, 0.10) samples (a) 0.1C rate, (b) 1C rate; (c) Comparison of the cycling performance of the Na_{1-x}Ca_{x/2}NFM (x=0, 0.05, 0.10) electrodes at 1C rate.

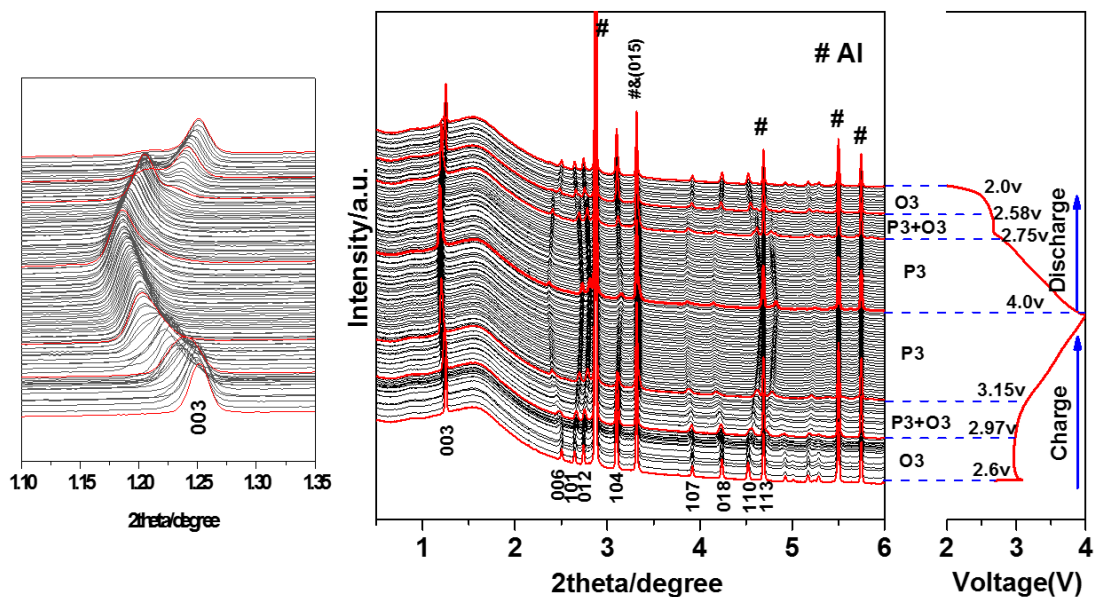


Figure 4. In situ XRD patterns collected during the first charge/discharge of Na_{0.9}Ca_{0.05}NFM electrode under 0.1C over a voltage range of 2.0-4.0 V.

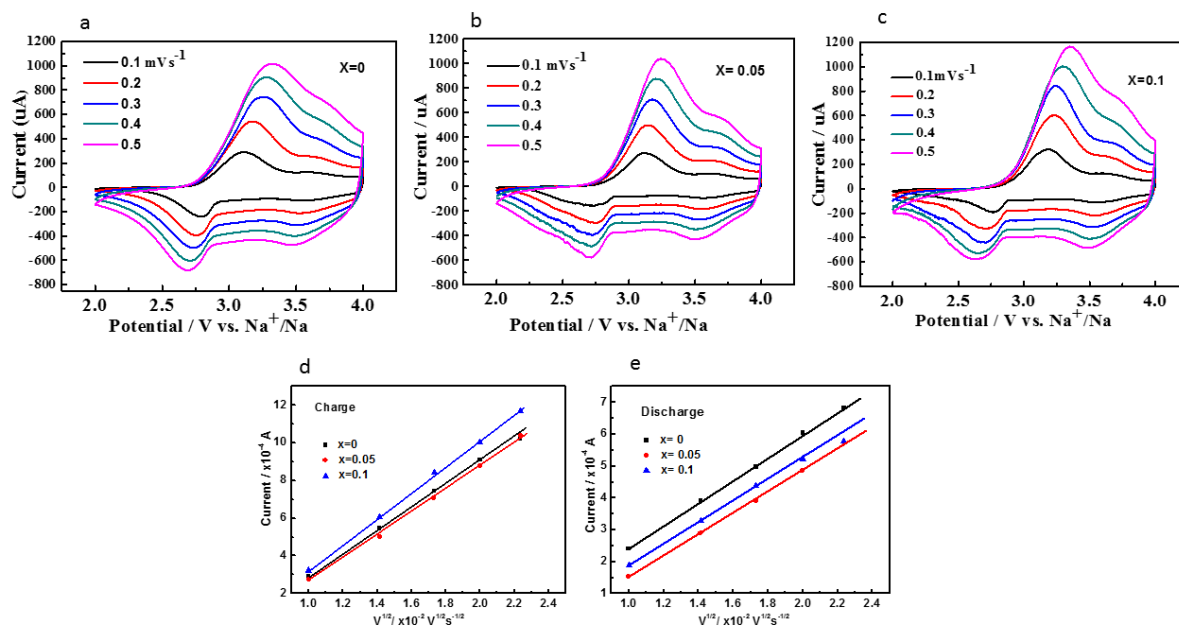


Figure 5. The CV curves of $\text{Na}_{1-x}\text{Ca}_{x/2}\text{NFM}$ (a) $x=0$, (b) $x=0.05$ and (c) $x=0.1$ in the potential window of 2.0–4.0 V vs. Na^+/Na at varied scan rates of 0.1, 0.2, 0.3, 0.4 and 0.5 mV s^{-1} . The dependence of peak current on the square root of the scan rate ($V^{1/2}$) for the $\text{Na}_{1-x}\text{Ca}_{x/2}\text{NFM}$ ($x=0, 0.05, 0.10$) electrodes during (d) charge and (e) discharge process.

Table 1. The calculation results of Diffusion coefficient values from varied CV curves for $\text{Na}_{1-x}\text{Ca}_{x/2}\text{NFM}$ ($x=0, 0.05, 0.10$) materials.

$\text{Na}_{1-x}\text{Ca}_{x/2}\text{NFM}$	Charge		Discharge	
	Slope(10^{-4})	$D(10^{-11}\text{cm}^2\text{s}^{-1})$	Slope(10^{-4})	$D(10^{-12}\text{cm}^2\text{s}^{-1})$
$x=0$	0.06167	1.36	0.03580	4.58
$x=0.05$	0.06040	1.43	0.03370	4.46
$x=0.1$	0.06800	1.82	0.03434	4.43

Effects of Ca-substitution in Na sites on the structural and electrochemical properties of $\text{Na}_{1-x}\text{Ca}_{x/2}\text{Ni}_{1/3}\text{Fe}_{1/3}\text{Mn}_{1/3}\text{O}_2$ ($x=0, 0.05, 0.1$) are investigated. All the samples show a single O3 type $\alpha\text{-NaFeO}_2$ structure with slightly increased alkali-layer distance as Ca content increased. The cycling stabilities of Ca-substituted samples are remarkably improved due to excellent structure recoverability after cycling.

Keywords: layered sodium transition metal oxide, sodium ion battery, Ca-substitution

Liqi Sun#, Yingying Xie#, Xiao-Zhen Liao*, Hong Wang, Guoqiang Tan, Zonghai Chen, Yang Ren, Jihyeon Gim, Wan Tang, Yu-Shi He, Khalil Amine, Zi-Feng Ma

Insight into Ca-substitution effects on O3-type $\text{NaNi}_{1/3}\text{Fe}_{1/3}\text{Mn}_{1/3}\text{O}_2$ cathode materials for sodium ion batteries application

